Surface & Coatings Technology 437 (2022) 128350

Contents lists available at ScienceDirect

Surface & Coatings Technology

journal homepage: www.elsevier.com/locate/surfcoat

Combined experimental-numerical analysis of the temperature evolution and distribution during friction surfacing

Zina Kallien [a,*], Benjamin Klusemann [a,b]

[a] Helmholtz-Zentrum Hereon, Institute of Materials Mechanics, Solid State Materials Processing, Max-Planck-Straße 1, 21502 Geesthacht, Germany
[b] Leuphana University of Lüneburg, Institute of Product and Process Innovation, Universitätsallee 1, 21335 Lüneburg, Germany

ARTICLE INFO

Keywords:
Friction surfacing
Finite element method
Temperature profiles
Dissimilar aluminum alloys
Solid state layer deposition

ABSTRACT

Friction surfacing (FS) is a solid state coating technology for similar and dissimilar metallic materials. The coating of the substrate with a consumable material is enabled due to frictional heat and plastic deformation and is performed below the materials' melting temperature. In this work, the spatio-temporal temperature field during FS is investigated within the substrate via a combined experimental-numerical approach. The study presents a robust and efficient thermal process model accounting for the contributions of friction and plasticity as heat input. The geometry of the applied heat source is dependent on the deposit geometry and the evolving flash. Extensive spatial temperature measurements for a dissimilar aluminum alloy combination are used in order to identify the required input parameters and to validate the model. The process temperature profiles for varied process parameters, such as axial force, rotational speed and travel speed as well as substrate thickness and backing plate material are systematically investigated, where experimental and numerical results are in good agreement. Deviations are in particular associated with possible experimental scatter and unknowns regarding the exact position of the measurement as well as modeling assumptions in terms of the heat source geometry. Overall, the detailed comparisons illustrate that the developed numerical model is able to obtain the temperature evolution and distribution during FS deposition with acceptable accuracy for a wide range of process conditions.

1. Introduction

The friction surfacing (FS) process is a coating technology enabling the deposition of a consumable material on a substrate due to frictional heat and plastic deformation. Since the materials remain in solid state throughout the whole process, the heat input is lower compared to fusion-based techniques. Therefore, the heat affected zone (HAZ) is reduced and large distortions are prevented [1]. So, solid state joining processes offer an alternative to conventional techniques based on material fusion for various metallic materials [2], where dissimilar combinations as e.g. aluminum on steel are also possible [3]. Furthermore, Huang et al. [4] showed that joining of aluminum and titanium is feasible by applying a hybrid approach of FS assisted by friction stir welding. The thermal loads during FS lead to microstructural changes in both substrate and deposited consumable material [5]. The thermo-mechanical input results in a fine grained microstructure of the coating material enabled by dynamic recrystallization [6]. The FS technique also allows to deposit multiple layers over or next to each other, suitable as approach for additive manufacturing (AM) [7–9]. In this regard, to make full use of the potential of FS, a detailed understanding of the temperature evolution and distribution during FS has to be achieved. The complex relation of material properties, process parameters and process environment with temperature and its effect on the resulting structure has to be solved.

Applied axial force, rotational and travel speed are the three main process parameters that significantly influence the deposit geometry as summarized and discussed, for instance, in the review by Gandra et al. [10]. Since the required energy input for the process is strongly dependent on the materials thermal properties [11], the choice of materials to be welded is fundamental for the selection of process parameters. The process parameters determine the energy input and directly influence the temperature evolution [12–14], which in turn affects the resulting microstructure and deposit geometry. In preliminary studies, the authors proposed a linear relation between process temperature and deposit geometry [15]. However, experimental temperature measurements are complex and typically limited to specific positions, where a numerical model allows the gapless analysis of temperature data at any point within the structure.

* Corresponding author.
E-mail address: zina.kallien@hereon.de (Z. Kallien).

https://doi.org/10.1016/j.surfcoat.2022.128350
Received 16 December 2021; Received in revised form 1 March 2022; Accepted 9 March 2022
Available online 15 March 2022

Compared to the knowledge about FS from numerous experimental studies, e.g. summarized in the review by Gandra et al. [10], the amount of numerical investigations of the FS process seems comparably rare. Gandra et al. [10] discuss the varying material properties for the plasticized material, the unknown friction coefficient and the asymmetric material flow as challenges that have to be faced for the development of FS process models. A physical model based on the theory of contact melting was developed by Liu et al. [16] in order to study the deposition mechanism. Temperature measurements with thermocouples in the consumable stud showed that the temperature at the interface between consumable rod and substrate is just below the melting temperature. In a further study, Liu et al. [17] presented a model based on finite difference to determine the thermal field in the consumable rod during deformation and plasticizing. Similarly, the evolving thermal field in the substrate material during plasticizing and deposition on was modeled subsequently by the same authors [18]. A finite element (FE) model, also developed by Liu and co-workers [19], showed that the consumable rod material at the rubbing interface plasticizes first and the highest strain occurs near the consumable stud's center on the bottom surface. A study by Vitanov and Javaid [20] presents a FE thermal model showing a good agreement with temperature measurements for the initial dwelling phase as well as during the deposition phase of the process. The validated model was used to predict the temperature at the rubbing interface and shows the effect of machine parameter variation on the calculated temperature at the materials' interface. Recent studies [13,14,21,22] also show good agreements of numerical models for selected single positions of temperature measurements performed during FS, which allow a detailed analysis of heating and cooling cycle for a single location but missing a high resolution analysis and comparison of temperature distribution along the substrate.

The focus of the present study is to develop a thermal process model in order to obtain the evolving temperature distribution during the process for different FS process configurations. Not only process parameters, i.e. rotational speed, applied axial force and travel speed, but also variation in substrate thickness and backing material are investigated, which was rarely done before, however, these parameters affect the process temperature as well as the deposit geometry [15]. Key aspect of the thermal modeling approach is a model for the heat source, which is proposed in this study based on experimental observation, i.e. the dimensions of the deposit. In order to validate the numerical model, experimental data providing high resolution temperature measurements across the substrate material is used. In this regard, the proposed model is validated not only at single selected positions but rather over a large area in the substrate material, allowing to obtain the evolving temperature distribution for different FS process configurations.

2. Experimental setup

To enable the deposition by FS, a consumable stud material is positioned above the substrate. A rotational speed and an axial force are applied on the stud which is pressed onto the substrate's surface. Friction and plastic deformation occur and lead to a sudden temperature increase at the interface. As a result, the tip of the stud deforms and starts to plasticize. When a relative translational movement between plasticized stud and substrate is superimposed, a layer of the plasticized stud material is deposited on the substrate. As a discontinuous process limited by the consumable stud's length, the deposition ends with stopping the relative translational movement between stud and substrate and the retraction of the remaining stud material.

The experiments of this study were performed on a custom-designed friction welding system RAS (Henry Loitz Robotik, Germany). The system has a working area of 0.5 m × 1.5 m and allows to apply forces up to 60 kN, torque up to 200 Nm and rotational speed up to 6000 rpm. During the experiments, the welding equipment is recording force and displacement in x-, y- and z-direction as well as values for rotational speed and torque. In the experiments, AA 5083 H112 stud material (20 mm diameter, 125 mm length) was deposited on AA 7050 T 7451 substrates (300 mm length, 130 mm width, 8 mm to 20 mm thickness) with different settings in process parameters, i.e. axial force, rotational speed and travel speed. Furthermore, the test conditions were varied, i.e. different substrate thicknesses as well as backing plates. The material for the backing plates between substrate and machine table was either AA 7050 (300 mm length, 130 mm width, 8 mm thickness or 300 mm length, 100 mm width, 12.5 mm thickness) or Ti64 (300 mm length, 100 mm width, 10.2 mm thickness). An overview of the performed experiments is given in Table 1. The FS process parameter configuration No. 1 is taken as reference process in the following. The experiments were originally performed by Kallien et al. [15] with the focus on identifying a correlation between deposit geometry and maximum process temperature for different process configurations.

Eight holes of 1 mm in diameter were drilled from the backside into the substrates ending 0.5 mm below the substrate's surface. The holes are evenly distributed from the center of the substrate in steps of 5 mm, Fig. 1, where one thermocouple (Type K) was positioned in each hole. The temperature was recorded at a frequency of 50 Hz. The dense distribution of the measurement points allows the analysis of the temperature evolution during FS across the deposited layer width from advancing side (AS) to retreating side (RS). The FS deposition process was initiated 70 mm before the measurements points and stopped 70 mm behind the measurement points resulting in 140 mm of total welding distance. In Fig. 1, the average maximum temperature values at eight positions from three experiments performed at same conditions are illustrated. The included errorbar, representing the difference of the average value to minimum and maximum temperature value for this position within the three experiments, is very small showing the robustness of the experimental setup.

For the analysis, optical analysis and imaging of the deposited structures was performed with a VHX-6000 digital microscope (Keyence, Germany) to obtain the deposit dimensions, i.e. average thickness and width. The values for the deposit geometry, as determined by Kallien et al. [15], are summarized in Table 3, including the measured stud feed rate. Furthermore, the cross sections of the deposits allow the analysis of the position of the deposited layer in relation to the substrate. Although, the positioning of the stud's center was always according to the substrate's centerline, the centerline of the resulting deposit does not correspond to the centerline of the substrate since the stud as well as the resulting deposit have a tendency to be deflected to the AS. Assuming that the material deposition is symmetric to AS and RS, the resulting centerline of the deposit can be determined as exemplarily shown in Fig. 1. The distance of the measurement positions to the determined centerline of the deposit was evaluated from the cross sections. For more details on the experimental setup and results, the interested reader is referred to Kallien et al. [15].

3. Numerical model

The temperature evolution during FS is characterized by a sudden temperature increase when the process is initiated. The frictional heat at the substrate-consumable stud-interface leads to deformation and plasticization of the stud. Since full-field experimental temperature data is rather limited, e.g. due to the limited number of thermocouples that can be positioned within the substrate material as well as the large experimental effort, a thermal process model allows a detailed analysis and a fundamental understanding of the temperature evolution and distribution within the full workpiece during the process.

In the current study, a heat transfer model was developed using the FE software LS-DYNA. The substrate and backing are modeled as solid parts of the same dimensions as used in the experiments[1] with an

[1] The holes which had to be drilled in order to perform temperature measurements experimentally are neglected in the model.

Table 1
Overview of experimental FS process setup for temperature measurements, corresponding to Kallien et al. [15].

Process no.	Axial force [kN]	Rotational speed [rpm]	Travel speed [mm/s]	Substrate thickness [mm]	Backing material
1 (reference)	8	1200	6	10	AA7050(8 mm)
2	8	1500	6	10	AA7050(8 mm)
3	8	900	6	10	AA7050(8 mm)
4	8	1200	8	10	AA7050(8 mm)
5	8	1200	4	10	AA7050(8 mm)
6	10	1200	6	10	AA7050(8 mm)
7	6	1200	6	10	AA7050(8 mm)
8	8	1200	6	8	AA7050(12.5 mm)
9	8	1200	6	12	AA7050(12.5 mm)
10	8	1200	6	16	AA7050(12.5 mm)
11	8	1200	6	20	AA7050(12.5 mm)
12	8	1200	6	8	Ti64(10.2 mm)
13	8	1200	6	12	Ti64(10.2 mm)
14	8	1200	6	16	Ti64(10.2 mm)
15	8	1200	6	20	Ti64(10.2 mm)

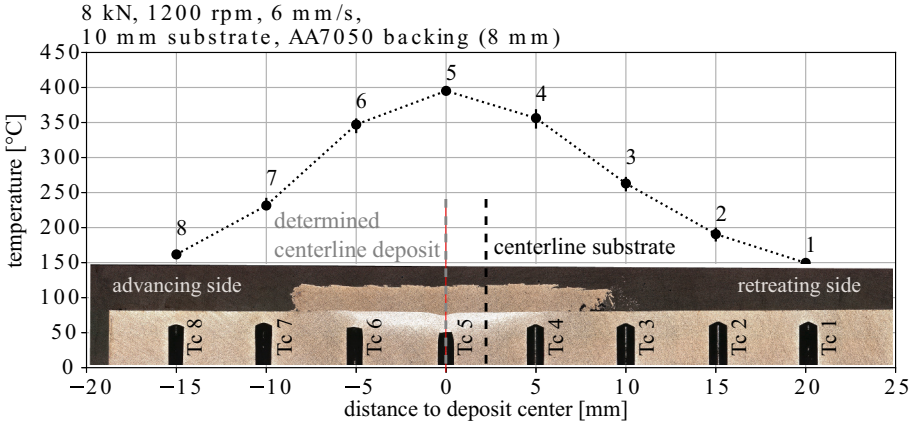

Fig. 1. Average maximum process temperatures at eight measurement positions for three individual deposition processes at 8 kN applied axial force, 1200 rpm rotational speed and 6 mm/s travel speed. The position of the measurements by thermocouples (Tc) was corrected according to the determined centerline of the deposit, however, the center of the stud was located according to the centerline of the substrate when starting FS. For more details see [15].

element mesh size of 1 mm in length and width direction. The mesh is biased in thickness direction, being very thin at the surface and coarser at the interface to the backing material, see Fig. 2. Substrate and backing material are bonded by merging the corresponding nodes. The nodes of the backing material's bottom surface are fixed in all degrees of freedom. On all surfaces of the model, heat radiation and convection are accounted for, assuming a surrounding temperature of 20 °C which equals the initial temperature of substrate and backing material. The coefficient value for convection is $h = 23 \frac{W}{m^2 K}$, and for emissivity $\varepsilon = 0.3$. The relevant material parameters used are shown in Table 2.

Similar to Liu et al. [19], the focus of this study lies on the simulation and understanding of the heat input to the substrate. Therefore, at this stage of investigation, a simplified heat flux model is developed without regard to other complex phenomena, e.g. behavior of the consumable stud material and the deposition of plasticized material. In this regard, the deposited material is neglected for simplicity in the heat transfer model. In order to simulate the heat input to the substrate during FS material deposition, a heat flux is applied to the top surface of the substrate material. The heat source travels the same path at the same travel speed as the stud in the experiments. For simplicity, the shape of the heat source used in this study is assumed symmetric,[2] Fig. 2.

[2] Within this study, the centerline of the deposits were determined as done by Kallien et al. [15]. The resulting maximum process temperature distribution with this correction is shown in Fig. 1. However, there is asymmetric material flow around the stud [10] that can hardly be determined precisely in order to be considered in a numerical model.

The source is assumed to consist of three parts. For the inner part, i.e. the center circle in Fig. 2, it is assumed that the consumable stud material is in direct contact with the substrate surface under the defined axial load. The radius r_c for the inner circle, representing the real contact plane during the process, see Fig. 3, is calculated following the approach by Fukakusa [25]:

$$r_c = \sqrt{\frac{d \cdot w \cdot v_{tr}}{\pi \cdot v_{cr}}}, \tag{1}$$

where d is the deposit thickness, w the deposit width and v_{tr} the travel speed. The feed rate, v_{cr}, is the average feed rate value during the deposition process. The values for the deposit geometry and the feed rate are taken from the experimental results [15] as summarized in Table 3. The heat which is applied in the contact area of the stud with the substrate, is calculated using an approach developed for friction stir welding (FSW) [26], adapted for the FS process. There are three main contributions determining the heat input: (i) the frictional heat due to the rotational movement, q_{rot}, (ii) the frictional heat due to the relative translational movement between substrate and consumable material, q_{tr}, and (iii) the heat due to plastic deformation of the material, q_{pd}. The heat input q_{rot} is calculated as follows:

$$q_{rot}(r, T) = \frac{2 \cdot \pi \cdot f \cdot \tau_{cp}(T) \cdot r_c^2 \cdot r}{A_{cp}}, \tag{2}$$

with the shear stress acting in the contact plane $\tau_{cp}(T) = \frac{F}{A_{cp}} \cdot \mu(T)$ and the real contact plane $A_{cp} = \pi \cdot {r_c}^2$. The process parameters, applied axial

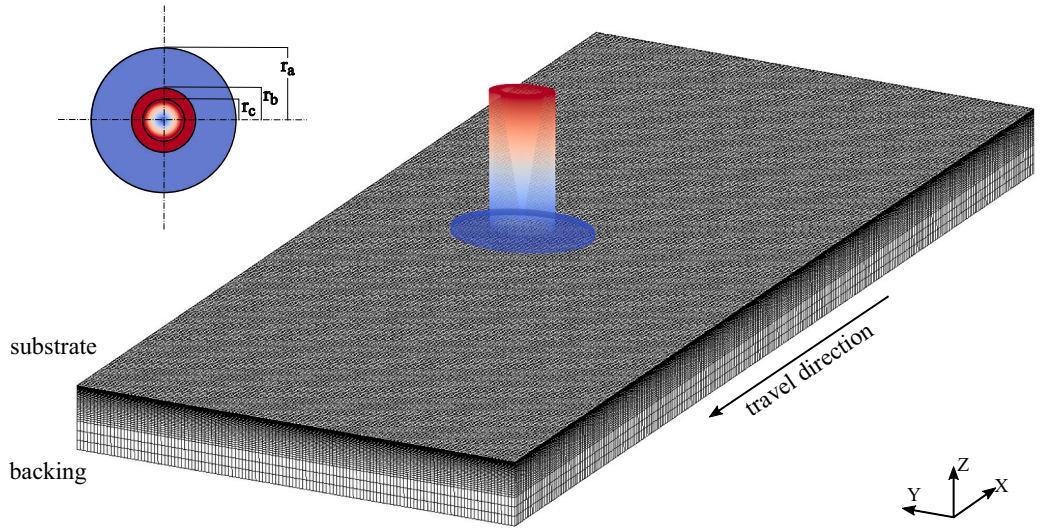

Fig. 2. Schematic of thermal model; the heat flux is applied to the surface of the substrate material.

Table 2
Material properties for AA 7050 [23] and Ti64 [24] used in the numerical model.

Material	Density	Specific heat	Thermal conductivity
AA 7050	2.83 $\frac{g}{cm^3}$	0.8600 $\frac{J}{gK}$	157 $\frac{W}{mK}$
Ti 64	4.43 $\frac{g}{cm^3}$	0.5263 $\frac{J}{gK}$	6.7 $\frac{W}{mK}$

force F and rotational speed f, determine the heat input. Furthermore, the applied heat of q_{rot} depends on the temperature-dependent friction coefficient $\mu(T)$ and the distance to the flux center r. This leads to larger heat input in the outer regions of this area due to higher tangential speed.

In general, the determination of the friction coefficient in solid state joining processes is very challenging [10]. In the present model an approach from FSW, e.g. used by Colligan and Mishra [27], is applied to calculate the initial friction coefficient μ_0 at temperature T_0 as

$$\mu_0 = \frac{3 \cdot M}{2 \cdot F \cdot r_c} \tag{3}$$

dependent on the average torque M and the applied axial force F, as well as the radius of the real contact plane r_c. Following the approach by Zhang et al. [28,29], the coefficient of friction is assumed to be temperature dependent as

$$\mu(T) = \mu_0 - K \cdot (T - T_0) \tag{4}$$

$$\text{with} \quad K = \frac{\mu_0}{T_{melt} - T_0}. \tag{5}$$

The main assumption of this approach is that the friction coefficient is linearly decreasing from μ_0 at T_0, 20 °C, to zero at T_{melt}, i.e. 629 °C for AA 7050 [23]. The second heat input due to friction is q_{tr}, calculated by

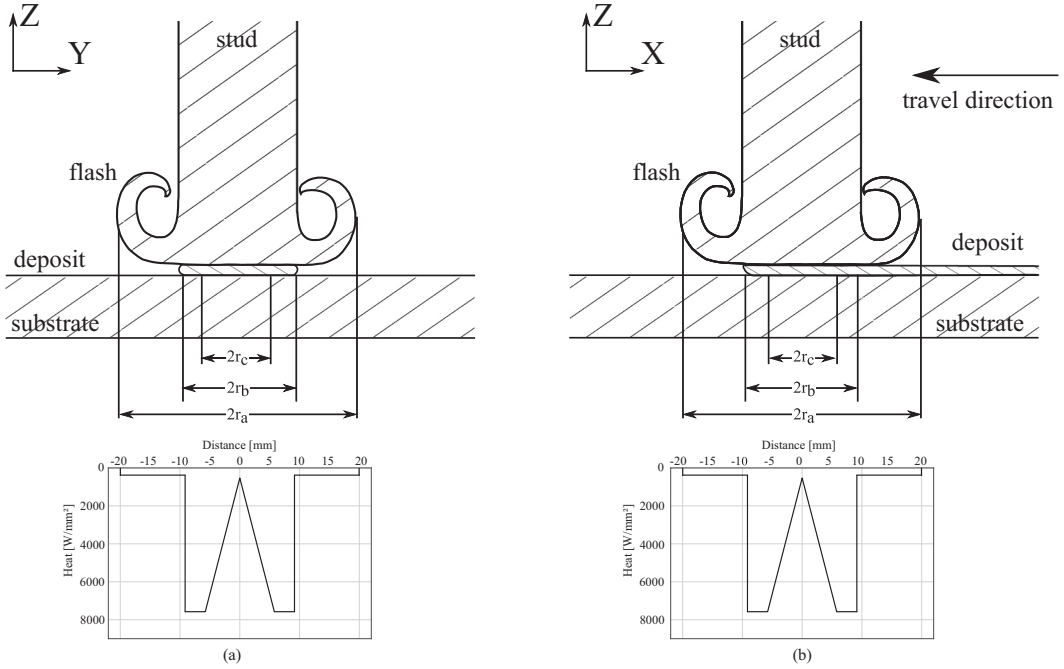

Fig. 3. Schematic of plasticized stud with flash, deposit and substrate during FS process and applied heat distribution.

Table 3
Overview of deposit geometry and average feed rate determined in the different processes, used to calculated r_c. The radius r_b is assumed to represent half of the deposit width. These values are used to determine the contributions in the heat source in the numerical model.

Process no.	Deposit thickness [mm]	Deposit width [mm]	Average feed rate [mm/s]	r_c [mm]
1 (reference)	1.75	18.30	1.83	5.78
2	1.40	16.86	1.83	4.96
3	2.33	19.26	1.86	6.79
4	1.69	17.77	2.18	5.92
5	2.15	19.06	1.93	5.20
6	1.64	19.10	2.44	4.94
7	1.99	17.12	1.43	6.75
8	1.92	18.16	1.93	5.87
9	2.19	17.89	1.99	6.14
10	2.24	18.15	2.03	6.18
11	2.30	17.72	2.16	6.01
12	1.51	19.01	1.77	5.57
13	1.99	18.60	2.01	5.93
14	2.02	18.27	2.07	5.84
15	2.20	18.06	2.01	6.14

$$q_{tr}(T) = \frac{\pi \cdot v_{tr} \cdot r_c^2 \cdot \tau_{cp}(T)}{A_{cp}}. \tag{6}$$

The third heat input due to plastic deformation of material, q_{pd}, is defined as

$$q_{pd}(T) = \frac{4 \cdot \pi \cdot f \cdot \tau_{pd}(T) \cdot d \cdot r_a^2}{A_{pd}} \tag{7}$$

with the shear stress $\tau_{pd}(T) = \frac{F}{A_{pd}} \cdot \mu(T)$, acting over the full radial area of the formed flash $A_{pd} = \pi \cdot {r_a}^2$.

As illustrated in Figs. 2 and 3, in this work the heat source can be subdivided into three regions. Within the inner region, representing the assumed real contact plane, all three heat contributions are acting, i.e.

$$q_{r_c}(r, T) = q_{rot}(r, T) + q_{tr}(T) + q_{pd}(T) \tag{8}$$

where the heat input increases with increasing radius to the stud center. The maximum heat input is reached at $r = r_c$, i.e.

$$q_{max}(T) = q_{rot}(r_c, T) + q_{tr}(T) + q_{pd}(T). \tag{9}$$

As experimentally observed, the calculated real contact area is significantly smaller than the actual area of the stud and the resulting deposit, i.e. determined by the deposit width. In this region, the stud material is no longer assumed to be in real contact during the process, i.e. no further frictional heat is created, however, the material is still fully deposited and in actual contact, i.e. a steady-state temperature within the deposited material is reached. Therefore, in this work, it is proposed that the required heat input to reach this temperature represents the heat input at r_c, q_{max}, which acts within the actual deposit area, i.e. r_b, represented by half of the deposit width, see Table 3. Therefore, the heat input between r_c and r_b, see Fig. 3, is assumed as

$$q_{rb}(T) = q_{max}(T). \tag{10}$$

Since in this model the material is not explicitly deposited, any temperature influence by the deposited material is assumed to be accounted for by the modeled heat source.

As it was noted by discrepancies between experimental measurements and numerical predictions for points relatively far from the deposition center, a further heat input outside the actual contact area is needed to accurately predict the temperature. Therefore, it is proposed that underneath the deformed stud material, represented by $2r_a$ in Fig. 3, a reduced constant heat input is acting. This reduced heat input is assumed to be a result of effects such as radiation as well as convection, since the gap between flash and substrate might be relatively small. The heat input in the area between r_b and r_a was assumed as

$$q_{ra} = \alpha \cdot q_{max}(T). \tag{11}$$

To illustrate the effect of the respective fitting constant α, the constant was varied from 0 to 15% of q_{max} and the results are presented for two points with different distance to the heat source center in Fig. 4. As

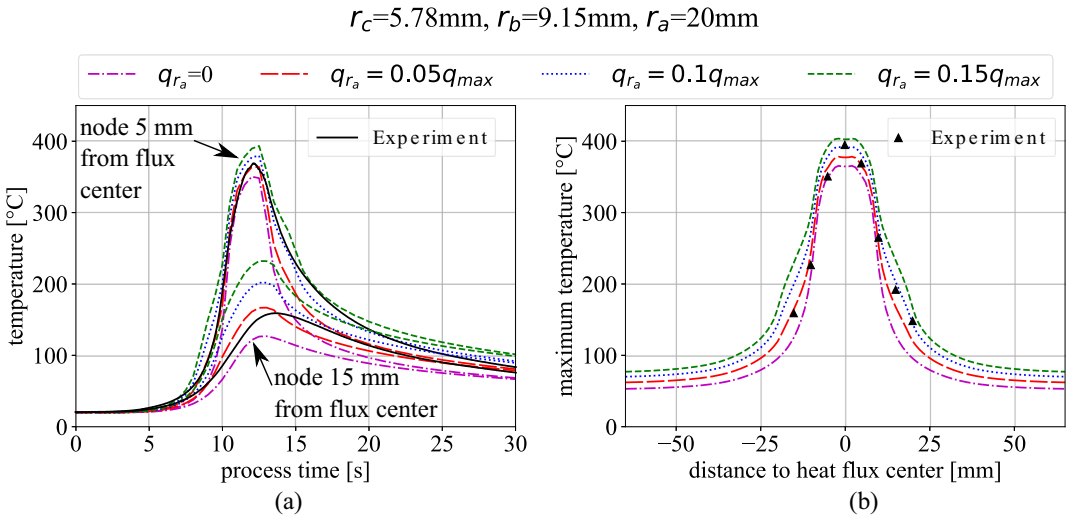

Fig. 4. Temperature curves for exemplary nodes 5 mm and 15 mm away from heat flux center (a), matching the measurement positions of Tc 8 and Tc 4 of the corresponding experiment (process No. 1), and maximum process temperatures along substrate's width (b) of numerical model for varied heat input in the area of r_a and the corresponding experimental data.

illustrated, the constant mainly effects the heat evolution far away from the center. As seen from these results, $\alpha = 0.05$ leads to the best fit to the experimental measurements for reference process, Table 1. This value for the fitting constant α is employed in all subsequent simulation results.

4. Results and discussion

4.1. Model behavior

In order to investigate and understand the model behavior with regard to changes of the heat source geometry, the different areas are varied independent of each other in the following. The main temperature influencing parameter of the heat source geometry is the corrected radius r_c of the assumed real contact area. The influence of variation of 1 mm in r_c, which equals a difference of approximately 17% to the reference process, is shown in Fig. 5(a) and (b). The effect of a r_c variation on the maximum process temperature distribution is limited to the center region. A decrease in r_c leads to increased temperature values in the center area because the heat input per area is increased.

Fig. 5(c) and (d) shows that a variation in r_b also has a significant influence on the general heating behavior and the distribution of maximum temperature. Increasing r_b leads to overall increased maximum temperature values and a wider temperature curve since the heat input within the circle ring between r_c and r_b is constant per area, but acts over a larger area. In this regard, the maximum process temperature distribution shows a strong gradient in the area between r_c and r_b.

Variations in r_a, Fig. 5(e) and (f), do not have significant impact since the heat in this area is comparably low. Only a slight change in the cooling behavior can be observed, leading to minimal changes of the maximum temperature distribution at the outer area of the heat source. The influence of the specific heat input value within this outer region is illustrated in Fig. 4. Since the effect of the variation in the geometry of r_a is not significant and limited to the outer region, in the following the value was assumed constant to $r_a = 20\ mm$, which is approximately the radius of the evolving flash. However, for other FS process configurations, which lead to significantly varying flash evolution, r_a might have to be adapted accordingly.

4.2. Comparison of numerical model and experimental data

In order to compare experimental and numerical results, the temperature curves and maximum temperature values are analyzed in the following. The experimental data, taken from the corrected measurement points, see Fig. 1, is compared to nodal data from the model, obtained at similar positions to those in the experiments.[3] Fig. 6 shows the temperature curves at different positions along the substrate's width for the reference process. In order to evaluate the sensitivity of the temperature to the exact measuring position, the heating rates for positions ± 1 mm and ± 2 mm in the model in relation to the reference nodal position are shown. The reference nodal position refers to the closest node corresponding to the measuring position in the experiment. The distance away from the heat flux center within the area of r_b is most critical for variations in the position matching thermocouples 3 and 7. For most deposits, these measurement positions are right next to the layer edges, see exemplary Fig. 1. For this position, 1 mm difference leads to a significant change in process temperature due to significantly different heat input, see Fig. 3. The other investigated positions are far less affected, even by a variation of ± 2 mm. Especially, the center node, matching the position of thermocouple 5 in the corresponding experiment, is very robust regarding the exact evaluation position. In the following analysis, the process temperature evolution for the position in the thermal model according to the experimental measurement position, including an uncertainty window of ± 1 mm, are shown in order to allow a valid comparison between experiment and simulation.

4.2.1. Influence of process parameter variation

Experimental measurements as well as the calculated temperature evolution for varied process parameters are shown in Figs. 7 to 9. The process parameters rotational speed and axial force are mainly determining the energy input whereas the travel speed defines the duration of the heat input. For the thermal model, the energy input in the outer area is assumed to be only 5% of the maximum generated heat. Therefore, the effect of any change in process parameters on the heat applied in this area is small compared to the other areas of the heat flux resulting in temperature values that are more or less independent from the changes in process parameters investigated. A change in process parameters is found to be crucial for the temperature values especially at the center positions of the deposit.

The results for varied travel speed are shown in Fig. 7. Numerical model and experimental data are in reasonable agreement. For high travel speed of 8 mm/s, a very fast heating can be observed by experimental and numerical results. For a low travel speed of 4 mm/s, a far slower heating and cooling can be observed, resulting in wider temperature curves and reaching higher maximum temperatures in the substrate material. With the calculated r_c values, which show a difference of 2% for 8 mm/s and 10% for 4 mm/s in comparison to the reference process, the heat source geometries and applied heat input are more similar for these two processes compared to the process parameter variations of applied axial force and rotational speed, which are discussed in the following.

In terms of rotational speed, higher temperature values are reached during the process in the center of the weld for higher rotational speed, Fig. 8. A variation of rotational speed influences the heat input directly and scales with the radius. The numerical results are overall in good agreement with the experiments. For the investigated rotational speeds, the resulting deposits showed very different dimensions leading to r_c values of 14% and 17% difference with regard to the reference process, respectively. Since the designed heat transfer model with the assumed real contact area, i.e. the calculated r_c, and its relation to the heat distribution during FS gives reasonable temperature distribution at eight positions in the substrate, it can be stated that the designed model is able to obtain the process temperature during FS.

An increase in axial force, e.g. from 6 kN to 10 kN, Fig. 9, leads to significantly higher temperatures at all measurements positions, resulting in relatively large changes of the deposit geometry, see Table 3. Consequently, the heat input and dimensions of the heat source in the processes at different axial forces are significantly different in the process model. The assumed real contact area is 15% lower for 10 kN and 17% larger for 6 kN compared to the reference process. The comparison of experimental and numerical results shows that for the 6 kN process, the model underestimates the temperature, whereas the temperature is overestimated for the 10 kN process. However, to reveal this effect further, the experiment of process No. 6, i.e. 10 kN, 1200 rpm and 6 mm/s, was repeated, revealing slightly different deposit dimensions[4] which were both considered in the process simulation. The results from both simulations are compared to the initially obtained experimental temperature curves for this process configuration, which is shown in Fig. 10. The comparison reveals that the slightly different values for r_c and r_b have already a considerable effect on the temperature curve determined by the thermal process model, where the slight changes lead to a remarkable better agreement with the experiment. The effect of

[3] The exact positions cannot be compared due to imprecise position of the deposit with regard to the thermocouples and the meshing in the finite element model.

[4] The repetition of process No. 6 revealed a deposit thickness of 1.80 mm, deposit width of 18.30 mm and average feed rate of 2.27 mm/s.

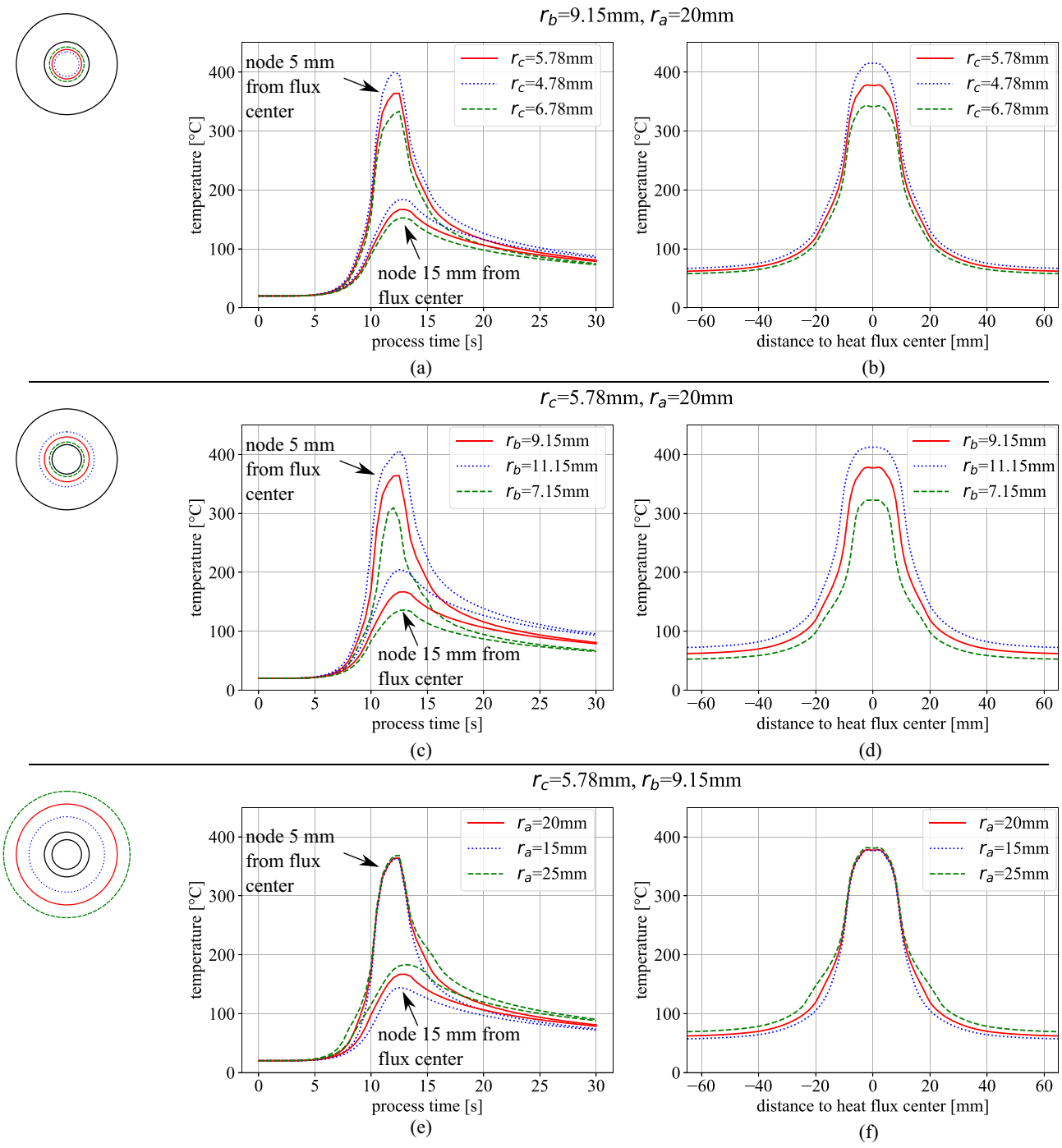

Fig. 5. Temperature curve for exemplary nodes 5 mm and 15 mm away from heat flux center (left) and maximum process temperatures along substrate's width (right) of numerical model for varied heat source geometries r_c (a)–(b), r_b (c)–(d) and r_a (e)–(f) using the remaining parameters of the reference process.

changing axial force or rotational speed is most pronounced within the area of deposited material, i.e. within r_b. In contrast, hardly any changes in temperature evolution or maximum temperature value could be observed for the positions further away from the heat source center.

For the investigation of process parameters, the observed trends with regard to maximum temperature are in agreement with the literature, e. g. [13,14]. Overall, the model is able to achieve a good agreement for the process parameter variation, in particular taking experimental scatter and possible uncertainties, e.g. in terms of the exact positioning, into account. The process parameters determine applied heat, heat source geometry and duration of heat input during FS process. Apart from a few exceptions, which might be related to measurement uncertainties, the thermal model is able to obtain the temperature evolution along the substrate's width for all process parameter variations in acceptable accordance to the experiments.

4.2.2. *Influence of substrate thickness and backing material variation*

The variation of substrate thickness was performed using AA 7050 backing plate, Fig. 11, as well as using a Ti64 backing plate, Fig. 12, keeping the process parameters constant at 8 kN applied axial force, 1200 rpm rotational speed and 6 mm/s travel speed, see Table 1. The different conduction conditions led to different deposit geometries, resulting in different values of r_b and r_c, see Table 3, and affecting the heat source dimensions. The r_c value, i.e. the dimension of the assumed

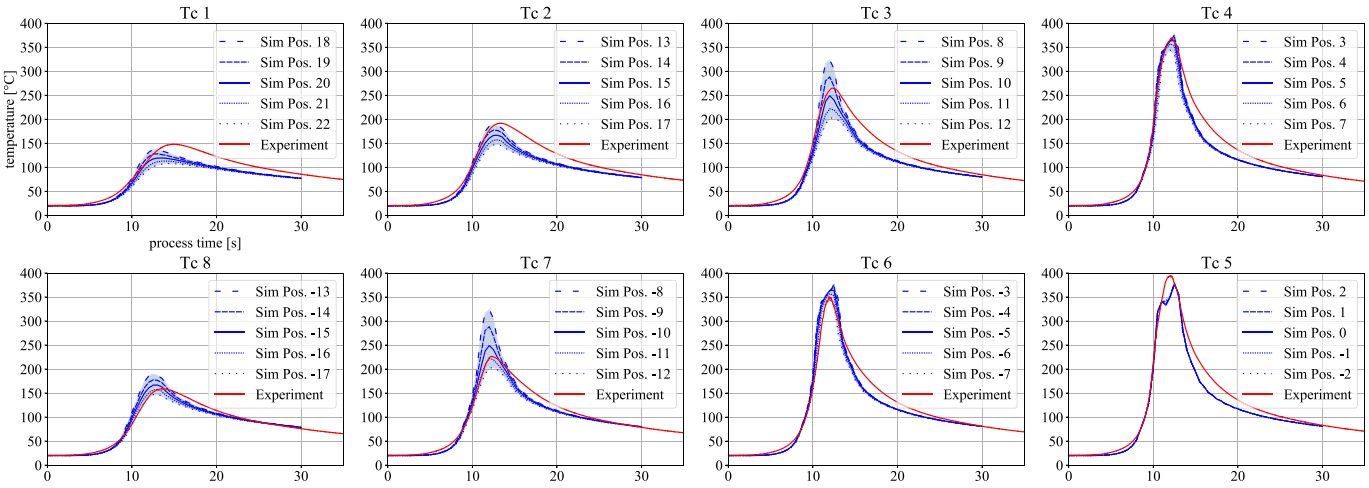

Fig. 6. Experimentally (Exp.) and numerically (Sim.) determined temperature evolution for process No. 1 (8 kN, 1200 rpm, 6 mm/s, 10 mm substrate, AA7050 backing plate). The solid lines show the process temperature at the nodes according to the corrected positions from the associated experiment; temperature evolution for the nodes ±1 mm (densely dashed/dotted lines) and ±2 mm (loosely dashed/dotted lines) show the difference of the model to account for uncertainties in the exact position of the thermocouple in the experiment as well as FE meshing.

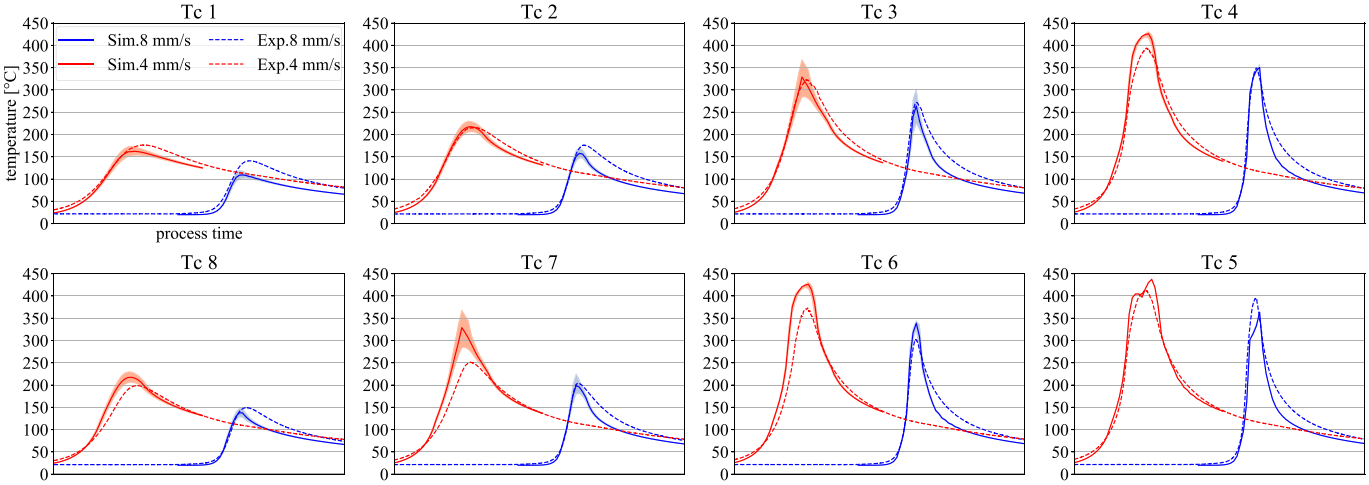

Fig. 7. Comparison of temperature curves of experiments (Exp.) detected by eight thermocouples and thermal model (Sim.) for variation of travel speed keeping all other parameters constant at 8 kN, 1200 rpm with 10 mm substrate and AA7050 backing, i.e. process No. 4 and 5.

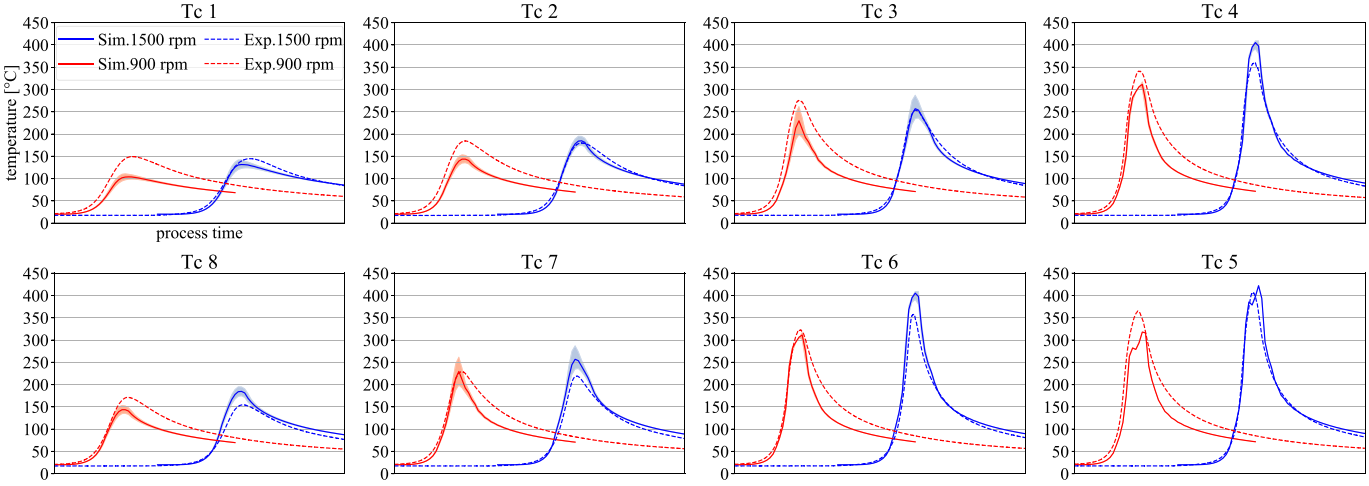

Fig. 8. Comparison of temperature curves of experiments (Exp.) detected by eight thermocouples and thermal model (Sim.) for variation of rotational speed keeping all other parameters constant at 8 kN, 6 mm/s with 10 mm substrate and AA7050 backing, i.e. process No. 2 and 3.

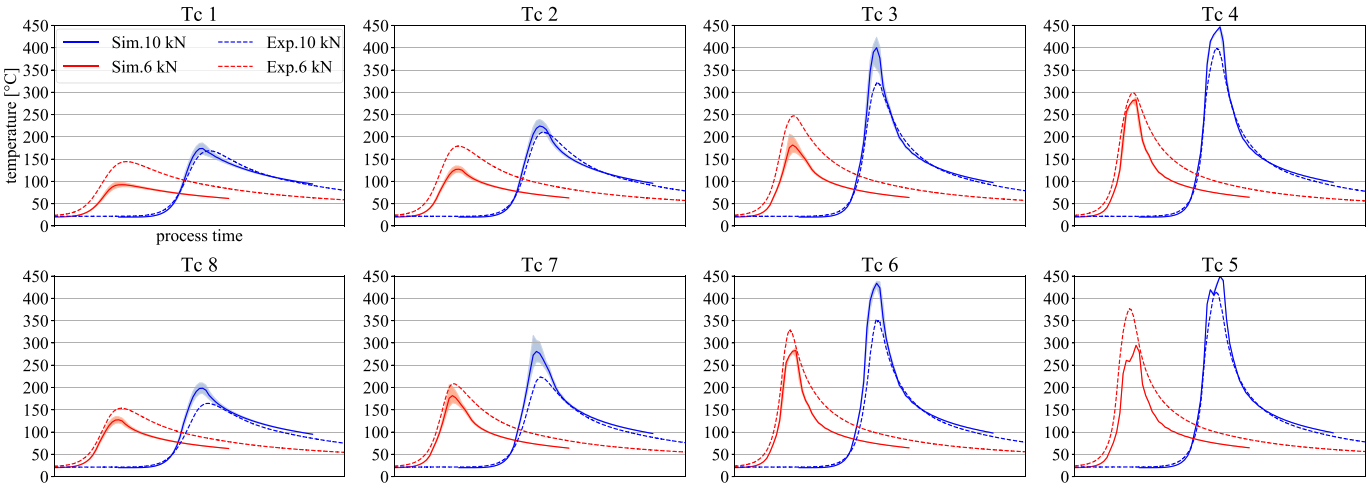

Fig. 9. Comparison of temperature curves of experiments (Exp.) detected by eight thermocouples and thermal model (Sim.) for variation of axial force keeping all other parameters constant at 1200 rpm, 6 mm/s with 10 mm substrate and AA7050 backing, i.e. process No. 6 and 7.

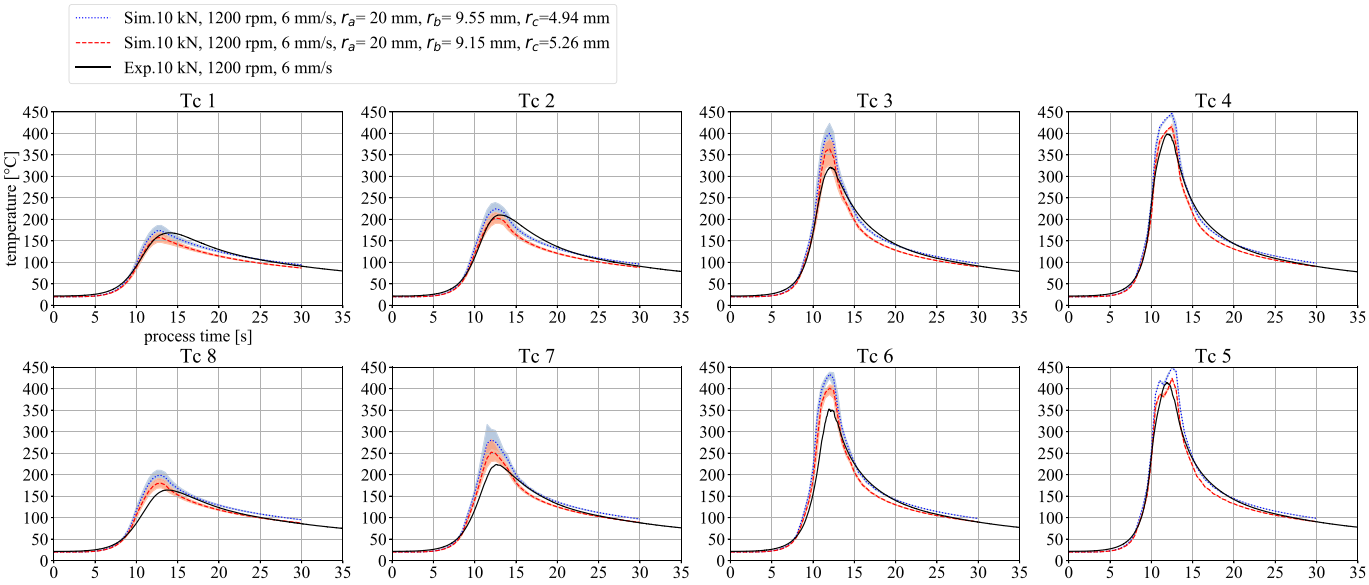

Fig. 10. Comparison of temperature curves of experiment (Exp.) detected by eight thermocouples and thermal model (Sim.) for 10 kN axial force, 1200 rpm rotational speed, 6 mm/s travel speed with 10 mm substrate and AA7050 backing, i.e. process No. 6, where the simulations are performed with different heat source dimension of r_c and r_b, according to measurements of two individual experiments.

real contact area, is between 5.43 mm and 6.18 mm for the variation in backing material and substrate thickness. The maximum difference to the reference process in terms of assumed real contact area of r_c is 7%, which is less compared to the previous process parameter variations. For most positions, the model determines a temperature evolution in good agreement to the experiments.

The thicker the substrate, the lower the maximum process temperature that was recorded during the deposition process. More heat can dissipate to thick substrates, whereas for very thin substrates, a heat build-up might occur. The use of a Ti64 backing plate leads to higher process temperatures compared to the AA 7050 backing plate, since the thermal conductivity of titanium is much lower. This effect is most pronounced for the substrates of 8 mm thickness. From the cross sections of the numerical model, Fig. 13, the effect of the backing material can be observed in detail along the substrate's thickness and length. Due to the lower thermal conductivity of the Ti64 backing material, there is a heat build-up in the substrate leading to higher process temperatures. Especially for the 8 mm substrate, the thermal model shows a faster cooling than the experiments. For thicker substrates of 12 mm, this effect is also observable but less severe. Obviously this difference between experiment and simulation is most distinctive for thin substrates and a Ti backing material. Possible deviations in the current simulations might be related to two reasons: First, the contact of substrate to backing is assumed ideal which is not the case during the experiments. Second, the built layer on the substrate surface is neglected. The deposition of warm plasticized material might have an effect on cooling behavior especially for thin substrates.

Overall, the developed thermal model shows very good agreement with experimental data for varied process parameters as well as substrate thickness and backing materials. The thermal model presents the heat distribution during FS, which can be very well obtained via the assumed contact area based on the deposit geometry. Sporadic deviations between simulation and experiment at specific measurement positions might be related e.g. to the uncertain positioning of the stud during deposition or deviations in the measurements. The results from the thermal model showed that the variation in process parameter,

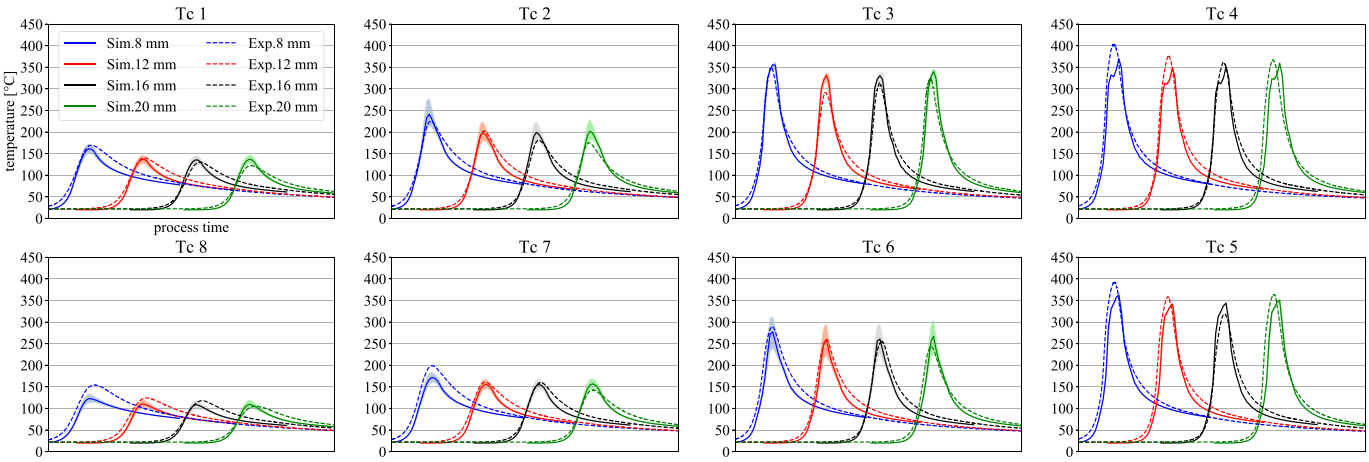

Fig. 11. Comparison of temperature curves of experiments (Exp.) detected by eight thermocouples and thermal model (Sim.) for variation of substrate thickness keeping all other parameters constant at 8 kN, 1200 rpm, 6 mm/s with 8 mm to 20 mm substrate thickness and AA7050 backing, i.e. process No. 8 to 11.

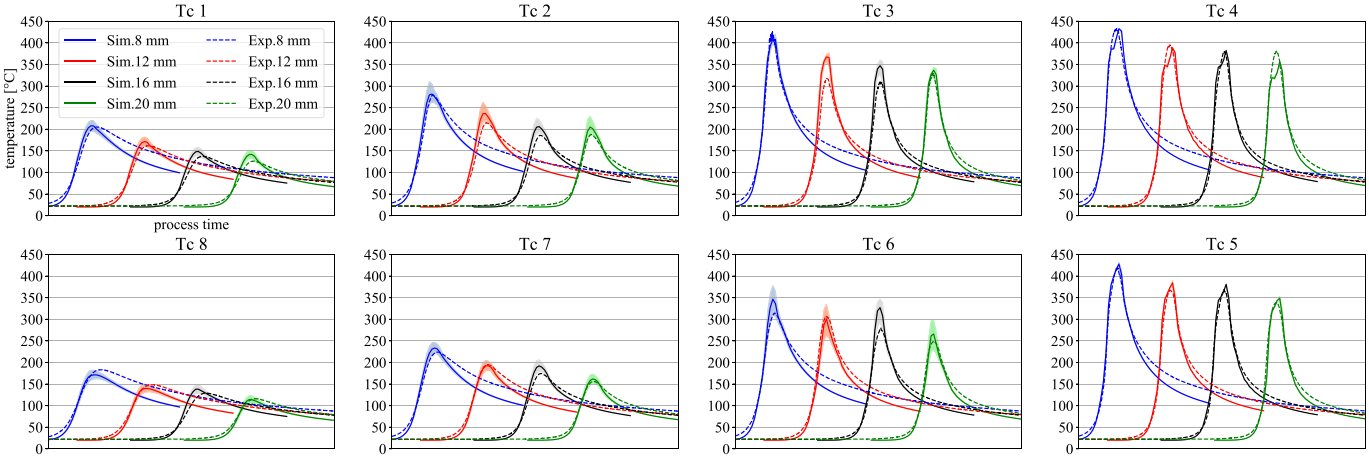

Fig. 12. Comparison of temperature curves of experiments (Exp.) detected by eight thermocouples and thermal model (Sim.) for variation of substrate thickness keeping all other parameters constant at 8 kN, 1200 rpm, 6 mm/s with 8 mm to 20 mm substrate thickness and Ti64 backing, i.e. process No. 12 to 15.

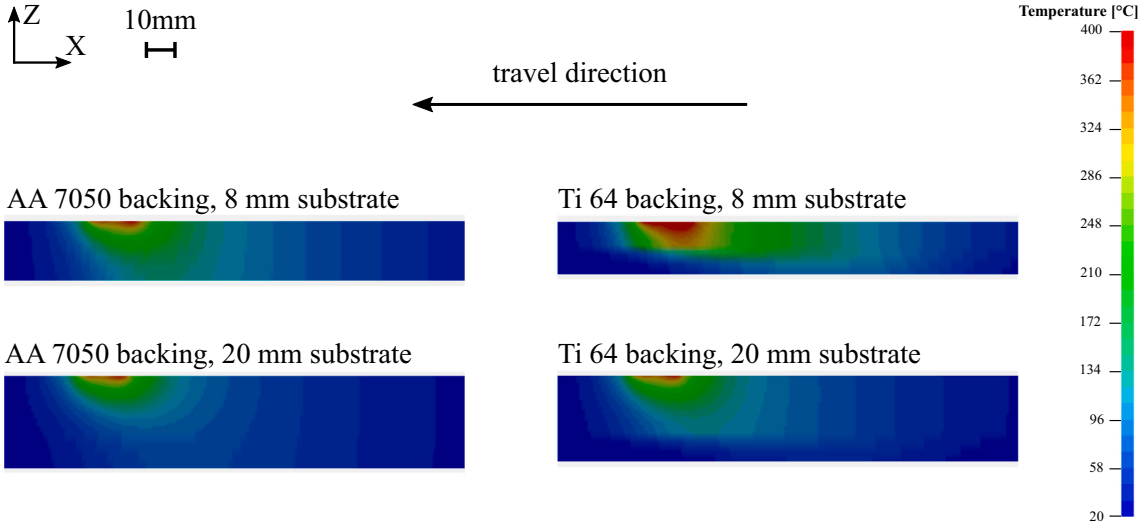

Fig. 13. Temperature distribution along substrate length and thickness at time $t = 15$ s; cross section at half of substrate's width for substrate thickness of 8 mm and 20 mm with Ti64 (10.2 mm) and AA7050 (12.5 mm) backing plate.

substrate thickness and backing material lead to different assumed real contact areas during the deposition process which is one main influencing factor when numerically obtaining the temperature evolution and distribution. Experimental studies showed that deposit geometry is in direct relation with process temperature and not solely defined by choice of process parameters [15], which is highlighted by the finding that external cooling also has an effect on deposit geometry [30]. The findings from the developed heat transfer model underline the relation of the temperature distribution at the deposit-substrate-interface and the deposit geometry.

5. Conclusion

In the presented experimental-numerical study, a thermal process model was developed to obtain the temperature evolution and distribution within the substrate material during FS deposition. The heat input to the substrate is determined by the process parameters, where the heat source shape was developed based on the geometry of the resulting deposit and the evolving flash. It is shown that the assumed contact area that evolves during the deposition process between consumable and substrate material is one key factor for the heat distribution and the resulting process temperature. Overall, the developed numerical model is robust for the FS deposition process and allows a detailed analysis of the temperature evolution and distribution for various FS process configurations, i.e. variation in process parameters as well as substrate thickness and backing material. Higher FS process temperatures are obtained for increase in axial force or rotational speed as well as for decreased travel speed. Higher process temperatures are also present when the substrate thickness is reduced or a backing plate material of lower thermal conductivity is used. Finally, the designed heat transfer model highlighted the relation of deposit geometry and temperature evolution and distribution in the substrate material during FS.

Funding

This project has received funding from the European Research Council (ERC) under the European Union's Horizon 2020 research and innovation programme (grant agreement No 101001567).

Data availability

The obtained data of this research is online available at Zenodo (DOI: 10.5281/zenodo.6355283).

CRediT authorship contribution statement

Z.K.: Conceptualization, Methodology, Validation, Formal analysis, Investigation, Data Curation, Writing-Original Draft, Writing-Review& Editing, Visualization; **B.K.:** Conceptualization, Methodology, Resources, Writing-Review& Editing, Supervision, Funding acquisition.

Declaration of competing interest

The authors declare that they have no known competing financial interests or personal relationships that could have appeared to influence the work reported in this paper.

References

[1] J. Gandra, R.M. Miranda, P. Vilaça, Performance analysis of friction surfacing, J. Mater. Process. Technol. 212 (8) (2012) 1676–1686.
[2] R.M. Miranda, J.P. Gandra, P. Vilaca, L. Quintino, T.G. Santos, Surface Modification by Solid State Processing, Woodhead Publishing in mechanical engineering. Elsevier Science, Burlington, 2013.
[3] H. Li, W. Qin, A. Galloway, A. Toumpis, Friction surfacing of aluminium alloy 5083 on DH36 steel plate, Metals 9 (4) (2019) 479.
[4] Y. Huang, Z. Lv, L. Wan, J. Shen, J.F. dos Santos, A new method of hybrid friction stir welding assisted by friction surfacing for joining dissimilar Ti/Al alloy, Mater. Lett. 207 (2017) 172–175.
[5] H. Khalid Rafi, K. Balasubramaniam, G. Phanikumar, K. Prasad Rao, Thermal profiling using infrared thermography in friction surfacing, Metall. Mater. Trans. A 42 (11) (2011) 3425–3429.
[6] U. Suhuddin, S. Mironov, H. Krohn, M. Beyer, J.F. Dos Santos, Microstructural evolution during friction surfacing of dissimilar aluminum alloys, Metall. Mater. Trans. A 43 (13) (2012) 5224–5231.
[7] J.J.S. Dilip, S. Babu, S.V. Rajan, K.H. Rafi, G.D. Janaki Ram, B.E. Stucker, Use of friction surfacing for additive manufacturing, Mater. Manuf. Process. 28 (2) (2013) 189–194.
[8] J.J.S. Dilip, G.D. Janaki Ram, B.E. Strucker, Additive manufacturing with friction welding and friction deposition processes, Int. J. Rapid Manuf. 3 (1) (2012) 56–69.
[9] J. Shen, S. Hanke, A. Roos, J.F. Dos Santos, B. Klusemann, Fundamental study on additive manufacturing of aluminium alloys by friction surfacing layer deposition, AIP Conf. Proc. 2113 (2019) 10015.
[10] J. Gandra, H. Krohn, R.M. Miranda, P. Vilaça, L. Quintino, J.F. Dos Santos, Friction surfacing—a review, J. Mater. Process. Technol. 214 (5) (2014) 1062–1093.
[11] S. Hanke, J.F. Dos Santos, Comparative study of severe plastic deformation at elevated temperatures of two aluminium alloys during friction surfacing, J. Mater. Process. Technol. 247 (2017) 257–267.
[12] V. Fitseva, S. Hanke, J.F. Dos Santos, Influence of rotational speed on process characteristics, material flow and microstructure evolution in friction surfacing of ti-6Al-4V, Mater. Manuf. Process. 32 (5) (2016) 557–563.
[13] P. Pirhayati, H. Jamshidi Aval, An investigation on thermo-mechanical and microstructural issues in friction surfacing of Al–Cu aluminum alloys, Mater. Res. Express 6 (5) (2019).
[14] Z. Rahmati, H. Jamshidi Aval, S. Nourouzi, R. Jamaati, Modeling and experimental study of friction surfacing of AA2024 alloy over AA1050 plates, Mater. Res. Express 6 (8) (2019).
[15] Z. Kallien, L. Rath, A. Roos, B. Klusemann, Experimentally established correlation of friction surfacing process temperature and deposit geometry, Surf. Coat. Technol. 397 (2020) 126,040.
[16] X.M. Liu, Z.D. Zou, Y.H. Zhang, S.Y. Qu, X.H. Wang, Transferring mechanism of the coating rod in friction surfacing, Surf. Coat. Technol. 202 (9) (2008) 1889–1894.
[17] X. Liu, J. Yao, X. Wang, Z. Zou, S. Qu, Finite difference modeling on the temperature field of consumable-rod in friction surfacing, J. Mater. Process. Technol. 209 (3) (2009) 1392–1399.
[18] X.M. Liu, Z.D. Zou, S.Y. Qu, J.S. Yao, Finite difference modeling on the temperature field of substrate in friction surfacing, in: 2010 Second International Conference on Computer Modeling and Simulation, 2010, pp. 360–364.
[19] X.M. Liu, Z.D. Zou, X.H. Wang, S.Y. Qu, Finite element analysis of the temperature field and strain field of coating rod in friction surfacing, Adv. Mater. Res. 97–101 (2010) 1433–1437.
[20] V.I. Vitanov, N. Javaid, Investigation of the thermal field in micro friction surfacing, Surf. Coat. Technol. 204 (16–17) (2010) 2624–2631.
[21] S.M. Bararpour, H. Jamshidi Aval, R. Jamaati, Modeling and experimental investigation on friction surfacing of aluminum alloys, J. Alloys Compd. 805 (2019) 57–68.
[22] F.Y. Isupov, O. Panchenko, L. Zhabrev, I. Mushnikov, E. Rylkov, A.A. Popovich, Finite element simulation of temperature field during friction surfacing of Al-5Mg consumable rod, Key Eng. Mater. 822 (2019) 737–744.
[23] MatWeb - Material property data: aluminum 7050-T7451 (7050-T73651) (Accessed 08.03.2021). URL http://www.matweb.com/search/datasheet_print.aspx?matguid=142262cf7fbc4c83917ca5c3d17df1ed.
[24] MatWeb - Material Property Data: Titanium Ti-6Al-4V (Grade 5), STA (Accessed 08.03.2021). URL http://www.matweb.com/search/DataSheet.aspx?MatGUID=b350a789eda946c6b86a3e4d3c577b39 ckck=1.
[25] K. Fukakusa, On the characteristics of the rotational contact plane – a fundamental study of friction surfacing, Weld. Int. 10 (7) (1996) 524–529.
[26] M.J. Russell, Development and Modelling of Friction Stir Welding, Dissertation, University of Cambridge, 2000.
[27] K.J. Colligan, R.S. Mishra, A conceptual model for the process variables related to heat generation in friction stir welding of aluminum, Scr. Mater. 58 (5) (2008) 327–331.
[28] X.X. Zhang, B.L. Xiao, Z.Y. Ma, A transient thermal model for friction stir weld. Part i: the model, Metall. Mater. Trans. A 42 (10) (2011) 3218–3228.
[29] X.X. Zhang, B.L. Xiao, Z.Y. Ma, A transient thermal model for friction stir weld. Part ii: effects of weld conditions, Metall. Mater. Trans. A 42 (10) (2011) 3229–3239.
[30] H. Krohn, S. Hanke, M. Beyer, J.F. Dos Santos, Influence of external cooling configuration on friction surfacing of AA6082 T6 over AA2024 T351, Manuf. Lett. 5 (2015) 17–20.